AIP | Advances

A novel 2nd-order bandpass MFSS filter with miniaturized structure

C. Y. Fang, J. S. Gao, and X. G. Feng

Citation: AIP Advances **5**, 087168 (2015); doi: 10.1063/1.4929722
View online: http://dx.doi.org/10.1063/1.4929722
View Table of Contents: http://scitation.aip.org/content/aip/journal/adva/5/8?ver=pdfcov
Published by the AIP Publishing

A novel 2nd-order bandpass MFSS filter with miniaturized structure

C. Y. Fang,[a] J. S. Gao, and X. G. Feng
Optical system Key Laboratory of Advanced Manufacturing Technology, Changchun Institute of Optics, Fine Mechanics and Physics Institute, Changchun, 130033, China

(Received 26 May 2015; accepted 10 August 2015; published online 24 August 2015)

In order to effectively obtain a miniaturized structure and good filtering properties, we propose a novel 2nd-order bandpass metamaterial frequency selective surface (MFSS) filter which contains two capacitive layers and one inductive layer, where there are multi-loop metallic patches as shunt capacitor C and planar wire grids as series inductor L respectively. Unlike the traditional operation way—the tuned elements used in resonant surface approximately equal to one wavelength in circumference and the structure thickness with a spacing of a quarter wavelength apart, by changing the value of L and C and matching multilayer dielectric to adjust the LC coupling resonance and the resonance impedance respectively, the proposed MFSS filter can achieves a miniatured structure with ideal bandpass properties. Measurement results of the fabricated prototype of the bandpass filter (BPF) indicate that the dimension of the tuned element on resonant surface is approximately 0.025 wavelength, i.e., 0.025λ. At the same time, the filter has the stable center frequency of f_0 = 1.53GHz and the transmittance of $T \geqslant 96.3\%$ and high Q-value for the TE/TM wave polarization at various incidence angles. The novel 2nd-order bandpass MFSS filter with miniaturized structure not only can decrease structure dimension, but also has a wide range of applications to microwave and infrared band. [http://dx.doi.org/10.1063/1.4929722]

I. INTRODUCTION

With the fast development of metamaterial and radar detection technologies in recent years, a lot of research into the bandpass filter (BPF) using artificially structured electromagnetic materials, known as metamaterials or composite materials, has attracted considerable attention.[1–4] As an artificially composite material which is composed of metamaterial and frequency selective surface (FSS), the metamaterial frequency selective surface (MFSS) can be used for the BPF applications because of its good frequency selective properties.[5,6] In general, frequency selective properties of the traditional BPF have to follow two basic principles. One is the tuned elements used in resonant surface approximately equal to one wavelength in circumference; another is the structure thickness equal to a spacing of a quarter wavelength apart. This can result in oversized structure and unwanted frequency properties.[7,8] Based on the traditional BPF, Seyed designed a harmonic-suppressed miniaturized-element BPF. By using multiple, closely spaced capacitive layers with overlapping unit cells to synthesize a single capacitive layer, the unit cell size was reduced effectively. Besides, the BPF has a fractional bandwidth of δ = 20% at 3GHz for TE/TM polarization and the ratio of wavelength vs. element dimension of λ/P = 4.17.[9] Mudar designed a synthesizing miniaturized element BPF containing the capacitive layer and inductive layer based on coupled resonators filter theory.[10] The BPF, as a function of incidence angle of the electromagnetic wave, has relatively stable operation frequency response of f_0 = 10GHz, fractional bandwidth of δ = 20% and λ/P = 5.36. However, it can be seen that whether the miniaturized-element BPF or

[a]f_y_u@sina.com

the coupled resonator BPF does not reach to better miniaturized feature and obtain ideal bandpass properties, such as less insertion losses and higher Q-value.

For this purpose, the paper proposes a novel 2nd-order bandpass MFSS filter containing two capacitive layers and one inductive layer, in which there are multi-loop metallic patches as shunt capacitor C and planar wire grids as series inductor L respectively. By changing the value of L and C and adjusting the coupled operation mode of C-L-C resonance circuit, the proposed BPF can operate under the resonance state. The principle of operation is to adjust the LC coupling resonance on capacitive layer and match inductive layer and multilayer dielectric impedance. Consequently, the dimension of the filter is decreased substantially. Measurement results indicate that the proposed BPF is feasible and applicable to microwave and infrared band. Compared to the existing BPF with the miniatured structure,[11–14] the novel BPF has not only better miniaturization characteristic, i.e., the dimension of the unit cell is 0.025λ (λ/P $\approx$ 200), but also good filtering properties for the TE/TM wave polarization at various incidence angles, such as a stable center frequency of f_0 = 1.53GHz and a transmittance of T = 96.3%.

II. DESIGN AND ANALYSIS

Figure 1 shows a general resonance circuit of the BPF, whose resonant frequency is determined by the formula:[15]

$$f = \frac{1}{2\pi\sqrt{L \cdot C}}, \tag{1}$$

where L and C are equivalent inductance and capacitance, respectively. Assuming the operation frequency of f_0 = 1.5GHz and the 0.025λ dimension of the tuned element 0.025, we can figure out the wavelength of λ = 200mm and the element dimension of P = 5mm. Thus, $L \bullet C = 1.13 \times 10^{-20}$H•F.

Here, we can design a novel circuit, as shown in Figure 2. By changing the value of L and C to adjust the circuit resonant mode of C-L-C coupled resonance, we can get the novel equivalent circuit model of the 2nd-order bandpass filter.

In the circuit, $Z_0 = 377\Omega$ is the free space impedance; the intrinsic impedances of the coupling mediums are $Z_1 = Z_0/\varepsilon_{r1}^{0.5}$, $Z_2 = Z_0/\varepsilon_{r2}^{0.5}$ and $Z_3 = Z_0/\varepsilon_{r3}^{0.5}$ respectively, while the efficient

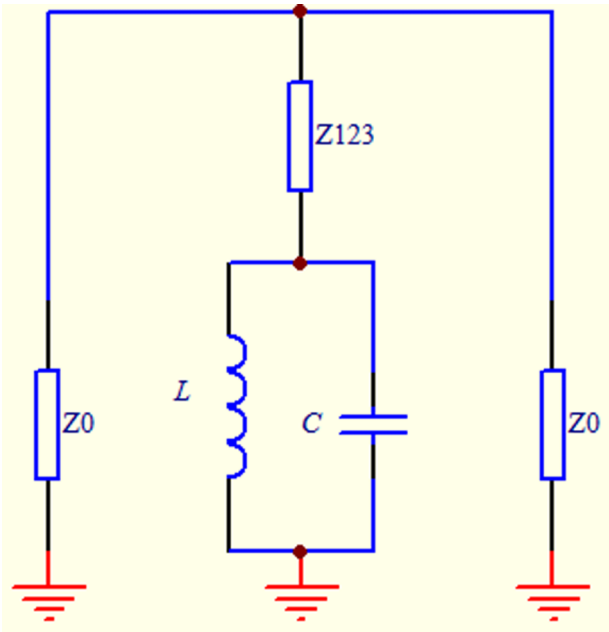

FIG. 1. A general LC resonant circuit.

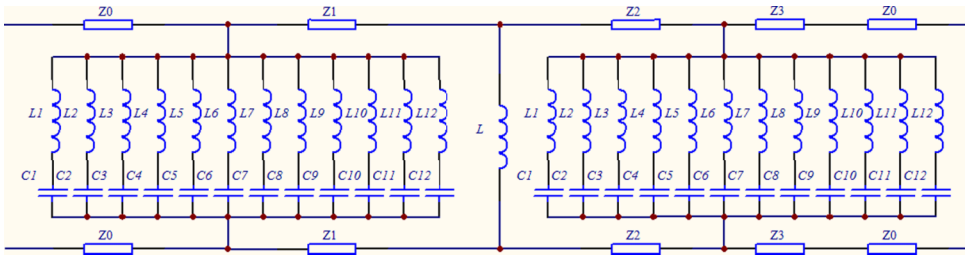

FIG. 2. Equivalent circuit model.

impedance of $Z_{123} = Z_1 + Z_2 + Z_3$. The capacitor and inductor value and of each capacitive loop patch is calculated by formulas:

$$\begin{aligned} C_i &= \varepsilon_0 \varepsilon_{eff} (2l/\pi) \ln (1/\sin (\pi S/2l)) \\ L_i &= \mu_0 \mu_{eff} (l/2\pi) \ln (1/\sin (\pi S/2l)) \end{aligned}, \tag{2}$$

where ε_0 and μ_0 are the permittivity and permeability of the free space respectively, where ε_{eff} is the effective permittivity of the medium in which the capacitive patches are located, μ_{eff} is the effective permeability of the medium in which the inductive wire grid is located, l is length of the wire grid. Accordingly, the impedance of each capacitor and inductor in series is expressed as:

$$Z_{CLi} = j\omega L_i + \frac{1}{j\omega C_i}. \tag{3}$$

Thus, the total impedance in C-L-C resonators, which are coupled to each other through series coupling inductors and the inductive layer, is calculated by formulas:

$$\frac{1}{Z_{CLC}} = \frac{1}{j\omega L} + \sum_{i=1}^{12} \frac{2}{j\omega L_i + \frac{1}{j\omega C_i}}. \tag{4}$$

According to the above formulas mentioned, we can calculate the parameters of the equivalent circuit. Further, based on the above, we can design the structure of the BPF filter. As shown in Figure 3, the BPF filter consists of the capacitive layers are modeled by shunt capacitors $(C_1, C_2 \ldots C_{12})$ and inductors $(L_1, L_2 \ldots L_{12})$, while the inductive layers are modeled by shunt inductors (L).

In addition, we need to analysis effects the multilayer dielectrics on incidence wave. As incidence wave going through the MFSS filter, the middle metal layer acted as an inductive surface corresponds to an inductor and stores magnetic energy. The coupling structures of the middle layer on top and bottom sides store electric energy and act as capacitive layer. The other layers in the structure are represented as transmission lines in the model, which are characterized by their impedance and electrical length. Next, we analyze the impedance and electrical length of multilayered dielectric as transmission lines in the model, in which the ganged transmission lines are connected to ports at each end to terminate the model with free space. When a plane wave is incident on a multilayered dielectric at various angles, the transmission line is related to a characteristic impedance and propagation constant, which depends on the incidence angle, frequency and polarization. The tangential components at the consecutive layers are related and the reflection and transmission coefficients of the total structure. As the angle of incidence of θ_i varies, the impedance of the wave within the dielectric is given by:

$$\begin{aligned} Z_{TE} &= \frac{Z_0}{\sqrt{\varepsilon_r} \cos \theta_r} \\ Z_{TM} &= \frac{Z_0}{\sqrt{\varepsilon_r}} \cos \theta_r \end{aligned}, \tag{5}$$

where ε_r and t is the dielectric constant of the dielectric layers and the thickness, as well as the index of refraction of $h = {\varepsilon_r}^{0.5}$; where Z_{TE} and Z_{TM} are the characteristic impedance for transverse electric

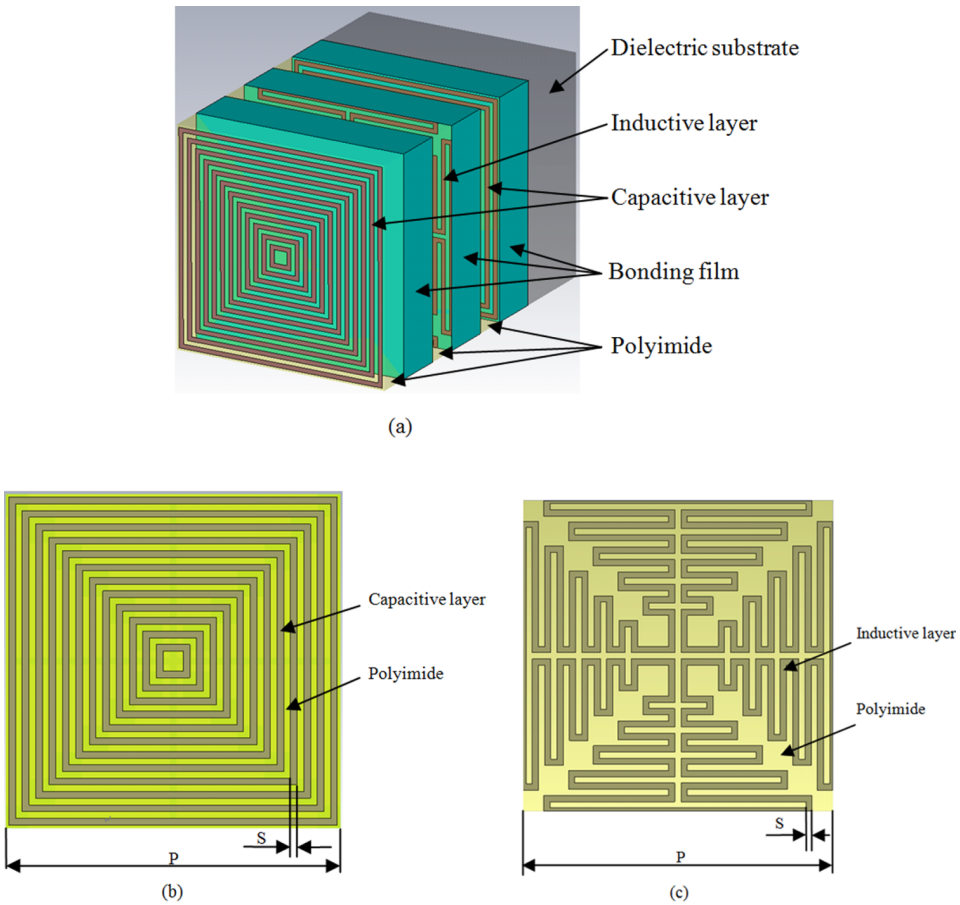

FIG. 3. (a): Structural diagram of the MFSS with (b): the multiple loops unit cell on the capacitive layer; and (c): the unit cell on the inductive layer.

(TE) and transverse magnetic (TM) incident fields; θ_r is the angle of the propagating wave passing through the dielectric. This angle is calculated using Snell's law of refraction and is given by:

$$\theta_r = \sin^{-1}\left(\frac{\sin\theta_i}{h}\right) \qquad h = \frac{\sin\theta_i}{\sin\theta_r} \tag{6}$$

Therefore, the shunt inductor and capacitor values of the circuit model are mapped to geometrical parameters. The equations presented above can be used to determine the impedance and

FIG. 4. Free-space measurement systems.

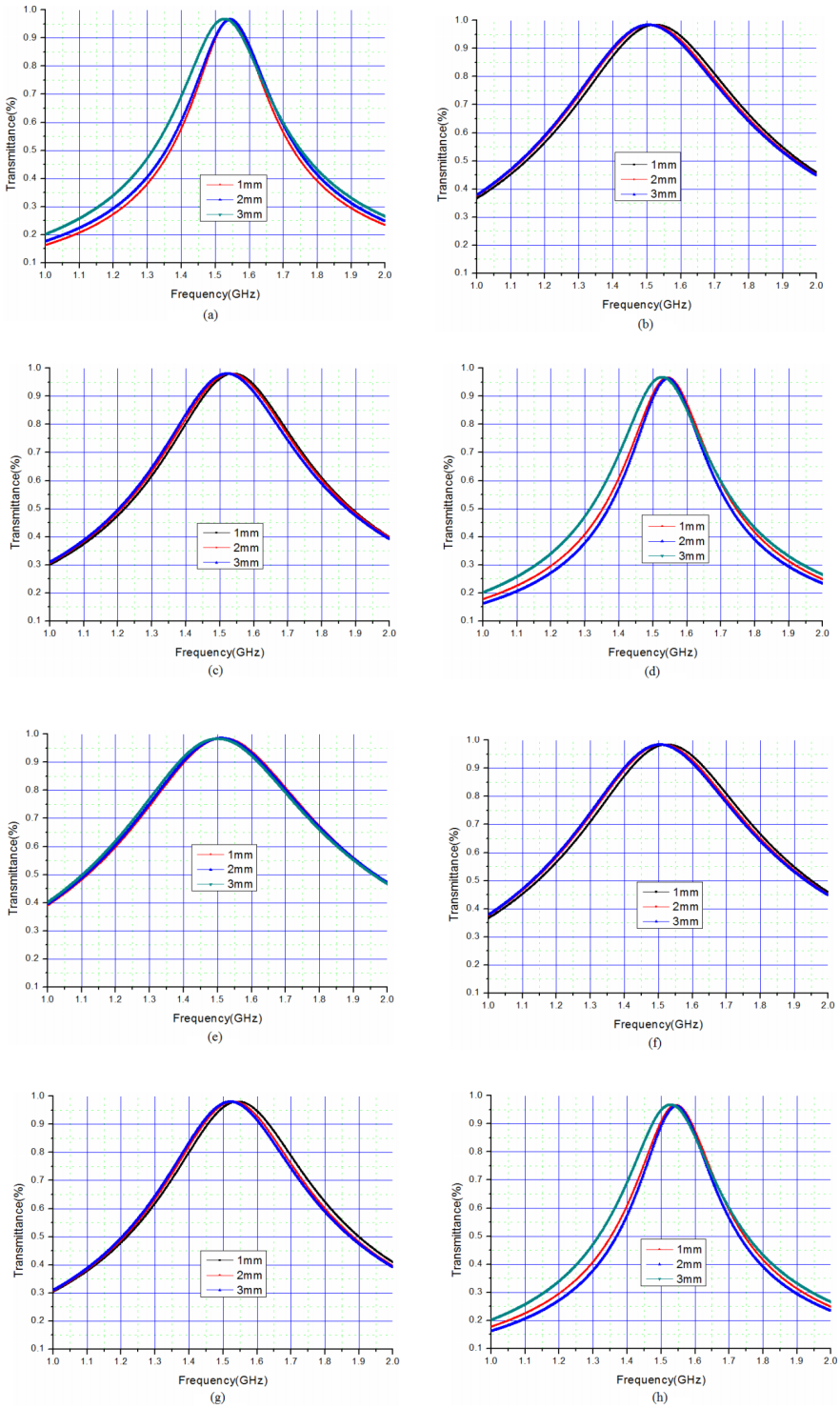

FIG. 5. Dielectric substrate ($\varepsilon_r = 3.17$) with different thickness for a: TE0°; b: TE20°; c: TE40°; d: TE60°; e: TM0°; f: TM20°; g: TM40°; h: TM60°.

electrical length of an arbitrary number of dielectric layers for TE and TM incident fields. The transmission coefficients of the total structure can be calculated for different polarizations and scan angles. The next is to study the bandpass properties of the MFSS filter for different polarizations and scan angles.

III. MEASUREMENT AND DISCUSSIONS

With knowledge of the incident angle for polarization wave and material properties, based on an equivalent circuit of representing the propagation through the multilayer materials, we can calculate the total load impedance of $Z_{CLC} = 693.46\Omega$ ($\varepsilon_{r3} = 3.17$) in C-L-C resonators, $L = 3.41$nH, $C = 3.31$pF. As shown in Figure 3, the proposed structure consists of three metallic layers (red copper) as the capacitive and inductive layers, which are placed on flexible polyimide and bonded with one dielectric substrate using bonding films. The capacitive layer consists of two-dimensional arrangement of metallic multi-square-loop patches with the width of S = 0.1mm, while the inductive wire grids are the combination of multi-T metallic strips with the width of S = 0.1 mm. The capacitive and inductive layers have the same periodicity of P = 5mm. The polyimide thickness $t_1 = 0.0254$mm, $\varepsilon_{r1} = 3.0$ and $\tan\delta_1 = 0.005$. As for bonding films, $t_2 = 0.04$mm, $\varepsilon_{r2} = 2.45$ and $\tan\delta_2 = 0.005$. As for the material parameters (ε_{r3}, t_3) of the dielectric substrate are determined according to the coupling status of the structure, assuming that the loss tangent value is $\tan\delta_3 = 0.008$. The fabricate prototype with the dimensions of 300mm × 300mm is measured in a free-space environment by using the vector network analyzer (Agilent N5244A), as shown in Figure 4. Besides the vector network analyzer, it comprises a pair of lens antenna, a bearing bracket and a rotatable table. By rotating the fabricated prototype 90 degree to change the direction of electric-field and the magnetic-field, we can easily measure the transmission characteristics of TE and TM wave illumination.

A. Effects of the dielectric substrate thickness

Figure 5(a), 5(b), 5(c), 5(d), 5(e), 5(f), 5(g), and 5(h) show the transmission properties of the structure with different thickness for the TE/TM polarization at incidence angles of 0°, 20°, 40° and 60° respectively. As can be observed in Table I, for the dielectric substrate ($\varepsilon_r = 3.17$) with thickness of t = 1mm and 3mm, the MFSS keeps mostly unchangeable center frequency of f_0 1.50-1.53GHz and a high transmittance of $T \geqslant 96.3\%$. For the TE/TM polarization at incidence angles of 20°/40° and the dielectric substrate thickness of t = 1mm, −1dB relative bandwidth and Q-value retain unchanged for 98% and 4.4 respectively. Compared with the result of 60°, −1dB relative bandwidth becomes bigger and Q-value becomes smaller. Similarly, so is the case with the dielectric substrate thickness of t = 3mm. It can be seen that the bigger −1dB relative bandwidth, the smaller Q-value. Besides, the dielectric substrate thickness has not effect on

TABLE I. Dielectric substrate ($\varepsilon_r = 3.17$) with different thickness.

T (mm)	Polar	θ	f_0 (GHz)	T	−1dB relative BW	Q
1	TE	0°	1.54	96.3%	9.7%	10.3
		20°	1.53	98.4%	22.9%	4.4
		40°	1.54	98.1%	23.3%	4.4
		60°	1.54	96.6%	10.5%	9.5
	TM	0°	1.52	98.5%	24.3%	4.1
		20°	1.53	98.4%	22.9%	4.4
		40°	1.54	98.1%	18.9%	5.3
		60°	1.54	96.6%	10.5%	9.5
3	TE	0°	1.53	96.9%	11.9%	8.4
		20°	1.51	98.4%	23.3%	4.3
		40°	1.54	98.0%	18.9%	5.3
		60°	1.53	96.9%	11.8%	8.4
	TM	0°	1.50	98.5%	24.8%	4.0
		20°	1.51	98.4%	23.3%	4.3
		40°	1.52	98.0%	18.9%	5.3
		60°	1.53	96.9%	11.9%	8.4

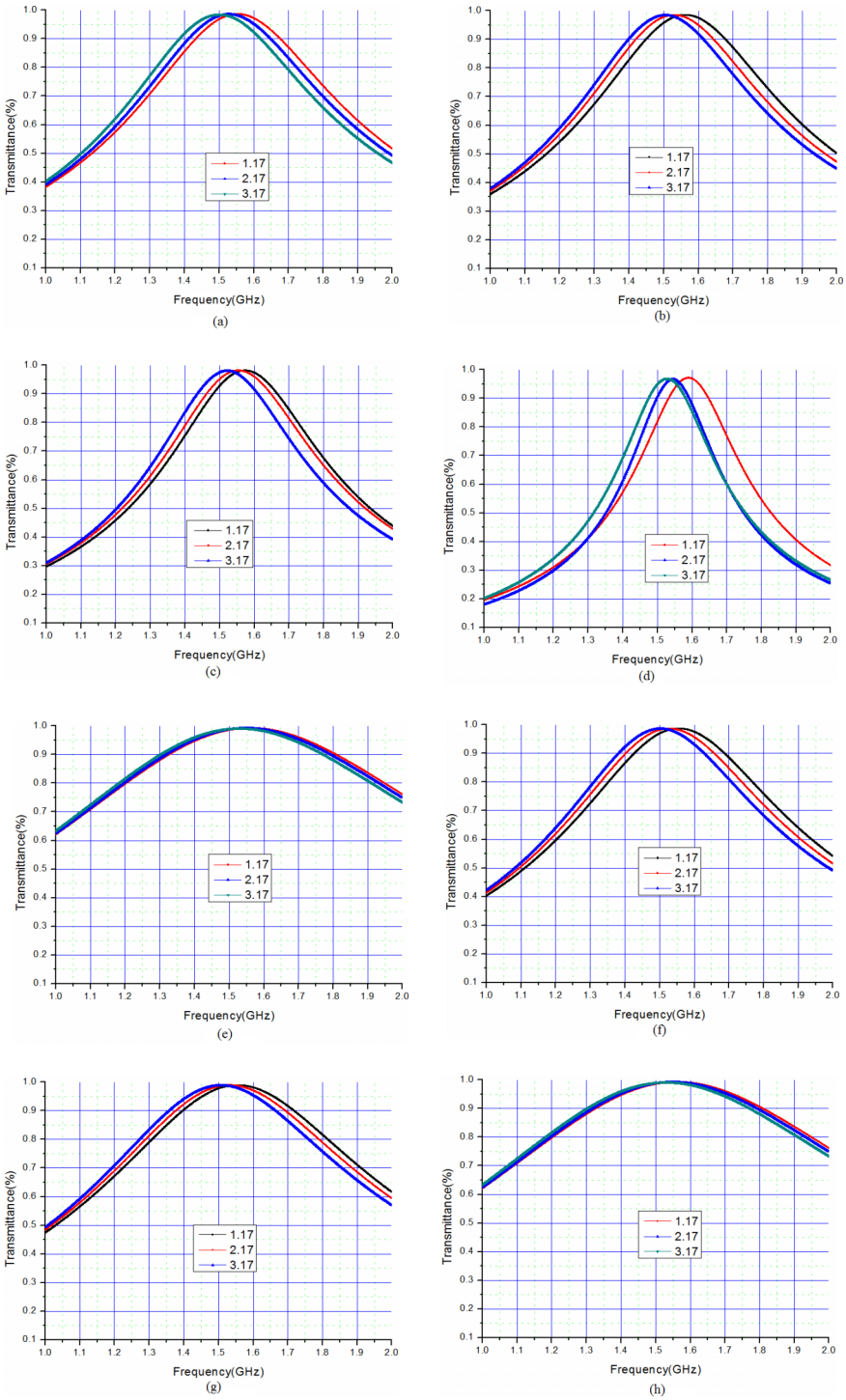

FIG. 6. Dielectric substrate with different dielectric constant for a: TE0°; b: TE20°; c: TE40°; d: TE60°; e: TM0°; f: TM20°; g: TM40°; h: TM60°.

transmission characteristics. Therefore, the proposed MFSS has a good filtering performance. This case results from mode matching variations of the parameters of the equivalent circuit model of the FSS under oblique incidence angles. Specifically, for the TE/TM polarization of incidence, the capacitance values of the patch layers decrease as the angle of incidence increases, while the inductance value of the wire grid does not change. At the same time, the series inductances—associated

TABLE II. Dielectric substrate with different dielectric constant.

ε_r	Polar	θ	f_0 (GHz)	T	−1dB relative BW	Q
1.17	TE	0°	1.55	98.6%	25.0%	4.0
		20°	1.6	98.5%	23.5%	4.2
		40°	1.57	98.1%	19.0%	5.2
		60°	1.56	99.2%	47.1%	2.1
	TM	0°	1.56	99.2%	47.1%	2.1
		20°	1.53	98.7%	26.6%	3.7
		40°	1.56	98.9%	32.4%	3.1
		60°	1.56	99.2%	47.1%	2.1
3.17	TE	0°	1.50	98.5%	24.9%	4.0
		20°	1.51	98.4%	23.3%	4.3
		40°	1.52	98.0%	18.9%	5.3
		60°	1.55	99.2%	47.1%	2.1
	TM	0°	1.53	99.2%	47.1%	2.1
		20°	1.50	98.6%	26.5%	3.8
		40°	1.51	98.8%	32.3%	3.1
		60°	1.55	99.2%	47.1%	2.1

with small transmission lines representing the dielectric substrates of the MFSS—increase as the incidence angle increases. These two effects compensate each other resulting in a stable center frequency of operation as the angle of incidence changes.

B. Effects of permittivity

Figure 6(a), 6(b), 6(c), 6(d), 6(e), 6(f), 6(g), and 6(h) (a) and (b) show the transmission properties measured of the structure with different permittivity for the TE/TM polarization at incidence angles of 0°, 20°, 40° and 60° respectively. As can be observed in Table II, as the dielectric constant of ε_r for the dielectric substrate (t = 3mm) shifting from 1.17 to 3.17, f_0 has changed a little from 1.50-1.60GHz, T exceeds 98%, and Q-value vary from 2.1 to 4.0. For this case we can do this analysis. The inductive layers are modeled by shunt inductors. The dielectric substrates separating the metallic layers are modeled by short pieces of transmission line with characteristic impedance of and length. The inductance of the wire grid in the middle layer decreases when the incidence angle increases, while the capacitance values of the patch layers do not change. The values of the series inductances representing the short transmission lines modeling the dielectric substrates decrease as the angle of incidence increases. The reduction of these inductance values results in increasing the center frequency of operation of the MEFSS for the TM polarization as the incidence angle increases.

Compared with the result of Table I, it can be seen that Q-value is on a downward trend. This shows that the dielectric constant of ε_r for the dielectric substrate has a great impact on Q-value when the incident wave is large angle.

IV. CONCLUSION

In this paper, the proposed MFSS filter has not only a minitured structure dimension, but also the expected bandpass properties such as the stable center frequency of f_0 = 1.53GHz and the transmittance of $T \geqslant 96.3\%$ for the TE/TM polarization at various incidence angles. The operation principle of the filter structure is different from the traditional operation way. It makes use of coupling two capacitive layers and one inductive layer to change resonance mode. By adjusting the value of L and C to change the coupled operation mode of C-L-C resonance circuit, we can obtain the expected bandpass properties. Measurement results indicate that the capacitance values of the patch layers can decrease as the angle of incidence increases, while the inductance value of the wire grid

does not change. The series inductances can increase as the incidence angle increases. These two effects compensate each other, which result in a stable center frequency of operation as the angle of incidence changes. Therefore, the novel 2nd-order bandpass MFSS filter has not only miniaturized structure and good transmission characteristics, but also a wide range of applications to microwave and infrared band.

ACKNOWLEDGMENTS

This work was supported by the national natural science foundation of China, No: 61172012. The author would like to thank Dr. Gao Jinsong for valuable advices regarding the investigation. In addition, I also thank Dr. Sun Lianchun and Feng Xiaoguo for critical reviews of the manuscript.

[1] NI Landy *et al.*, Phys Rev Lett. **100**, 207402 (2008).
[2] A. D. Boardman *et al.*, Laser Photon. Rev. **5**, 287 (2011).
[3] TT Yeh *et al.*, Optics Express **20**, 7580 (2012).
[4] X. P. Shen *et al.*, Optics Express **19**, 9401 (2011).
[5] G. Q. Luo *et al.*, IEEE Trans. Microwave Theory and Tech. **55**, 2481 (2007).
[6] M. Al-Joumayly *et al.*, IEEE Trans. Antennas Propag. **58**, 4033 (2010).
[7] S Barbagallo *et al.*, Electron. Lett. **42**, 382 (2006).
[8] F Huang *et al.*, Electron. Lett. **42**, 788 (2006).
[9] Seyed Mohamad Amin Momeni Hasan Abadi *et al.*, IEEE Trans. Antennas Propag. **62**, 2562 (2014).
[10] Mudar A. Al-Joumayly *et al.*, Antennas and Propagation Society International Symposium 1 (2010).
[11] E. A. Parker *et al.*, Electron. Lett. **44**, 394 (2008).
[12] H. L. Liu *et al.*, IEEE Trans. Antennas Propag. **57**, 2732 (2009).
[13] Cheng-Nan Chiu *et al.*, IEEE Antennas and Wireless Propagation Letters **8**, 1175 (2009).
[14] L. P. S. Campos *et al.*, Microwave Opt. Technol. Lett. **51**, 1983 (2009).
[15] Sanjeev Yadav *et al.*, *International Conference on Signal Propagation and Computer Technology* (2014).